

Enhancement in Entanglement Growth due to the Breaking of Translational Symmetry

Roopayan Ghosh and Arnab Das

School of Physical Sciences, Indian Association for the Cultivation of Science, Jadavpur, Kolkata-700032, India.

(Dated: May 15, 2022)

Information, unlike energy or matter, can leak out of a sub-system to its environment not only due to leaking out of particles from the sub-system to the environment, but also due to leaking in of particles to the sub-system from the environment. We show, this leads to a striking phenomenon – within a simple setup of free-fermions on a one-dimensional lattice, the breaking of the translational symmetry (TS) may lead to enhancement of information leakage from a sub-system to the environment, though the local correlations show slower propagation upon breaking of the TS as expected. We explain this enhanced leakage in terms of enhancement of entanglement between the sub-system and the environment due to additional scattering of the particles back into the system due to the broken TS. At its extreme, an enhanced leakage of information is observed on introduction of *random* on-site potentials, as long the size of the sub-system is of the order of the localization length. For weak disorder the localization length can be considerably large, and we provide a quantitative estimate of that, elaborating on the time and length scale in which this phenomenon is observed. Our counter-intuitive results will provide useful insights and caveats in designing secured local quantum information storage devices based on localization.

PACS numbers:

I. INTRODUCTION

Consider a local system storing information embodied in microscopic quantum degrees of freedom, e.g., spins or fermions. Now suppose there is a weak coupling between the system and its surrounding environment. The question of how fast and how much information can leak out of the system, can be modeled most simply within the setup of inhomogeneous quenches^{1–11}. An homogeneous quench refers to evolving a closed quantum system under a local Hamiltonian H , starting from an initial state (obviously not an eigenstate of H , but often the ground state of some other Hamiltonian) that breaks the translational symmetry (TI). Since the paradigm includes evolution of a bipartite system whose two different partitions are initialized to very different states, it is a natural setting for describing the evolution of a quantum information storage system initialized to a desired state, under the influence of its environment whose state can be quite generic. An elementary setup that mimics the scenario consists of free fermions on a one dimensional lattice, with a section of the lattice, i.e, a set of consecutive lattice points (the system), is entirely occupied by the fermions, while the rest (the environment) is completely empty (the domain wall state).

In our work we extend the study of the inhomogeneous quench with domain wall like initial conditions to systems where we have broken the Translation Symmetry(TS) by spatially varying the on-site potential. While there has been some study in this direction¹², we will show that as we break the translation symmetry and introduce a spatial inhomogeneity in the lattice, the Entanglement Entropy (EE) of the system may actually saturate to a higher value. This pattern of increase continues as we switch from periodic sequence to automated sequences

which have quasi-periodicity, e.g. Fibonacci sequence and finally go to random disordered systems, which shows highest Entanglement values. We will show how localization of the evolving many body state affects the EE. We discuss the reason behind the counter-intuitive result, viz. a higher density of particles arriving in the subsystem from the surroundings does not necessarily ensure a higher entanglement entropy in such quenches. This is vastly different from the known results for global or local quenches in such 1D fermionic systems, and to the best of the knowledge of the author, has not been previously studied rigorously in case of inhomogeneous quenches in existing literature.

Fig. 1 describes our quench in a schematic diagram and shows it's difference from a local quench. We take one system $X1Y1$ with a certain particle density and another system $X2Y2$ with a different particle density and then at $T = 0$ glue $X2$ and $Y1$ together and let the system evolve. The simplest case, which is the one considered here is when $n_{X1Y1} = 1$ and $n_{X2Y2} = 0$ where n denotes average particle density per site. This difference in particle densities will induce a flow of particle current which in turn creates entanglement between the two halves of the system. Equivalently, we can consider the full system $X1Y2$ and start with a domain wall initial state with a domain wall at $i = L/2$ separating $n = 1$ and $n = 0$ sectors. This picture may be more useful for qubit systems where one can start from such an initial state is present at time $T = 0$, if we use JW transformation to go from the spin 1/2 language to Fermionic language. Additionally, domain wall picture is easier to use for analysis and we will refer to it in rest of our work. This type of quench is neither a global quench since the state itself is not translationally invariant nor a local quench since the difference in energy of this state and the ground state of the Hamil-

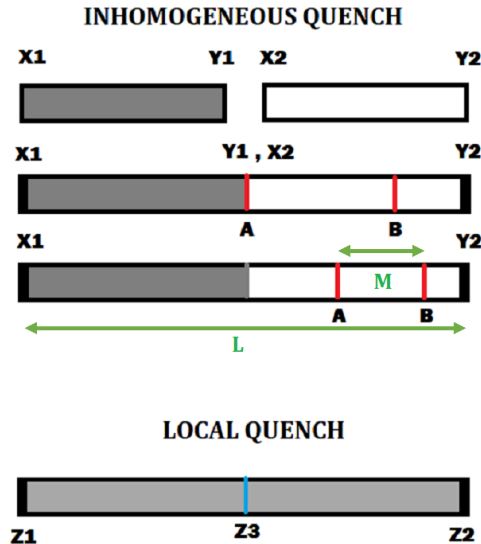


FIG. 1: (Colour online) A schematic diagram showing the case of inhomogeneous quench and its difference with local quench. In an inhomogeneous quench we take two systems $X1 Y1$ and $X2 Y2$ and glue $X2$ and $Y1$ together at $T = 0$. The system $X1Y1$ has a different filling fraction than $X2Y2$. The boundary conditions are open boundary conditions in each case. AB denotes the subsystem considered in the work. Notice that A denotes the leftmost site in the subsystem and B denotes the right most. In most cases, we take A to be exactly at $Y1(X2)$, but A can, in principle, be chosen anywhere in the system on the right. The system size is denoted as L and the subsystem size as M , which represents the number of sites in the lattice. In the last diagram we show the local quench scenario, where the blue line denotes a bond or site defect which is intensive in number. The system is allowed to evolve from this initial state, which is the ground state of the defect free Hamiltonian. See text for details.

tonian is extensive. It is expected the results will show features intermediate to both kinds of quenches. In this work however we show that the translation symmetry broken cases generate results completely different from the well known results for global and local quenches. This paper is arranged as follows, in Sec.II we discuss the Hamiltonian used in our simulations, and give a brief overview of the quantities involved in the calculations. Then in Sec. III, we discuss the various numerical results obtained for the different cases and give explanations for such behaviour, and finally in Sec. IV, we discuss the significance of the results obtained and possible implications.

II. DESCRIPTION OF THE MODEL AND QUANTITIES CALCULATED

Throughout the paper, the model Hamiltonian used for calculations is.

$$\mathcal{H} = -\frac{J}{2} \sum_m (c_m^\dagger c_{m+1} + c_{m+1}^\dagger c_m) + J \sum_m \mu_m c_m^\dagger c_m \quad (1)$$

where $c_m [c_m^\dagger]$ are fermion annihilation [creation] operators and μ_m is the on site potential which is either $\mu_0 + \delta\mu$ or $\mu_0 - \delta\mu$. The Hamiltonian is now scaled in units of J which is the hopping strength. We consider four distinct arrangements of μ_m .

1. Constant: In this scenario $\delta\mu = 0$, thus we have a translationally invariant system. For this case exact analytical calculations are available in literature^{3,5}. We provide a summary of the calculations in the supplementary material.
2. Periodic: We choose to work with two kinds of periodic potential. As the first example of a periodic potential, we choose $\mu_m = \mu_0 + (-1)^{\sum_{n=1}^L \delta_{m,np}} \delta\mu$. This represents a periodically varying potential with period p , in which every p^{th} site has a potential $\mu - \delta\mu$ and every other site has a potential $\mu + \delta\mu$. As a second example of a periodic potential we choose a square pulse like potential varying between $\mu_0 + \delta\mu$ and $\mu - \delta\mu$ with period q i.e.
$$\begin{aligned} \mu_m &= \mu_0 + \delta\mu, & m &= 1 \dots q/2 \\ \mu_m &= \mu_0 - \delta\mu, & m &= q/2 + 1 \dots q \end{aligned}$$
repeated over all the length of the lattice.
3. Automatic: A sequence is said to automatic or k-automatic if the n^{th} term in the sequence can be generated by a finite automaton by accepting the number n in base k .¹³ We will, in this focus on the Quasi-periodic sequence, Fibonacci word sequence, a short description of which is provided below. In the supplementary material, details and results for two more automated sequences, the Thue-Morse and Rudin-Shapiro sequence are discussed. A Fibonacci sequence is generated by the following recursion relation,

$$F_n = F_{n-1} + F_{n-2}$$

With $F_0 = 0$ and $F_1 = 1$. Thus the well known Fibonacci sequence looks like $0, 1, 1, 2, 3, 4, 8, 13, \dots$. Later, Chuan^{14,15} introduced a concept of Fibonacci words, defined on the alphabet set $\{0, 1\}$ in which the length of the n^{th} word in the sequence is given by F_n . These words are generated by the concatenation of the previous two words. Formally, $S_n = S_{n-1}S_{n-2}$ where S_n is the n^{th} Fibonacci

word. S_0 is taken to be 0 and $S_1 = 01$. Thus the first few terms of the words are,

$$\begin{aligned} S_0 &= 0 \\ S_1 &= 01 \\ S_2 &= 010 \\ S_3 &= 01001 \\ S_4 &= 01001010 \\ &\vdots \end{aligned}$$

Even at $N \rightarrow \infty$ it can be shown that S_N has no periodicity and the word is unique. However, it is clear that the letters(digits) in the word are correlated. The type of sequence in S_N has been labelled as a quasi-periodic sequence in literature. For a system of size L , where L is chosen to be a number in the Fibonacci sequence, we generate the Fibonacci word sequence and then define,

$$\begin{aligned} \mu_i &= \mu_0 - \delta\mu, & S_L^i &= 0 \\ \mu_i &= \mu_0 + \delta\mu, & S_L^i &= 1 \end{aligned} \quad (2)$$

where we have labelled the i^{th} letter(digit) in S_n as S_n^i .

4. Random: In this case, the potential on site μ_m is chosen randomly between $\mu - \delta\mu$ and $\mu + \delta\mu$. For numerical calculations averaging over several realizations of the random numbers is performed.

For our purpose we would consider a system with L -sites with open boundary conditions occupied by $L/2$ spinless fermions, with the initial condition,

$$\begin{aligned} \langle c_m^\dagger c_n \rangle &= \delta_{mn} & m \leq L/2 \\ &= 0 & \text{otherwise} \end{aligned} \quad (3)$$

Starting from $T = 0$, our aim is to study the evolution of Entanglement between the right half of the system with the left. We would calculate two quantities, Von Neumann Entropy and Mutual Information for this purpose. A short description of how each quantity is calculated is given below.

To calculate Von Neumann entropy, we first choose a subsystem of M sites. For most cases we would deal with a subsystem of $i = L/2 + 1$ to $i = L/2 + M$, i.e. a set of sites just to the right of the origin. We could have as well found the entanglement between $i = L/2$ to $i = L/2 - M + 1$ with the rest of the system and the results would be quantitatively equal. We would mainly discuss the case when $M = L/2$, i.e. the bipartite system since it is of physical interest in situations discussed in Sec. I Since we have a quadratic, particle conserving, fermionic Hamiltonian, all its eigenfunctions can be written as Slater determinants. Hence, one can write the Von Neumann entropy for an instant of time t as,^{16,17}

$$S_{vN}(t) = \sum_{i=1}^M \lambda_i(t) \log \lambda_i(t) + (1 - \lambda_i(t)) \log[1 - \lambda_i(t)] \quad (4)$$

where $\lambda(t)$ are the eigenvalues of $C_{mn}^{res}(t)$. $C_{mn}(t) = \langle c_m^\dagger(t) c_n(t) \rangle$ and $res.$ denotes indices restricted to the subsystem under consideration.

$\langle c_m^\dagger(t) c_n(t) \rangle$ can be exactly calculated for any value of time, using the Heisenberg picture. Since we are dealing with free systems, the expression can be written in terms of single particle eigenfunctions and eigenvalues as,

$$\begin{aligned} \langle c_m^\dagger(t) c_n(t) \rangle &= \sum_{k,l,i,j} U_{km} U_{ln} U_{ki} U_{lj} e^{i(E_k t - E_l t)} \times \\ &\langle c_i^\dagger(0) c_j(0) \rangle \end{aligned} \quad (5)$$

where E_k are the one particle eigenvectors and U is the Unitary matrix diagonalizing the one-particle sector of the Hamiltonian. For details, refer the supplementary material.

Mutual Information between two subsystems labelled by α and β is defined as follows,

$$\mathcal{M}^{\alpha\beta} = S_{vN}^\alpha + S_{vN}^\beta - S_{vN}^{\alpha\cup\beta} \quad (6)$$

Mutual Information gives an estimate of leakage of information from one subsystem to another.

III. RESULTS

Fig. 2 sums up the main result of this work. The top left panel shows the distribution of $\langle c_i^\dagger c_i \rangle$ at time $T = 500$ for characteristics potential in each of the types described in Sec II. $p = 1$ denotes the constant potential. The system size is taken to be $L = 2048$ for all the cases except Fibonacci series, as it is not a part of the Fibonacci sequence, and hence, one cannot form a Fibonacci word of that length. The closest Fibonacci word length is 2584 and that is what has been used. Hence the x axis is the rescaled site index as $x = (i - L/2)/L$. In each case we have chosen $\mu_0 = \delta\mu = 0.1$. For the Random sequence, we have simulated 60 disorder realizations. This is enough to get a very good idea about the qualitative nature of the plot since the system size under consideration is quite large and there is some self averaging. p and q denotes the two kinds of periodicities of two kinds of periodic potentials discussed. The top right panel shows the variation number density of particles in the region $i > L/2$ for the cases in the left panel. Both the plots point to the conclusion, the greater the inhomogeneity in the system, the slower the particles move. Thus the wavefront remains closer to the $i = L/2$ region and the number density is lowest in the case we have disorder. Quasi-periodicity and periodicity similarly affects the distribution but has a progressively lower effect. This is further shown by the fact $p = 16$ shows a lower value of n_{tot} than $p = 2$ case, this is because the eigenspectrum of $p = 2$ case is closer to $p = 1$ case than $p = 16$. It also shows the two kinds of periodicities show similar results qualitatively. For more details regarding various

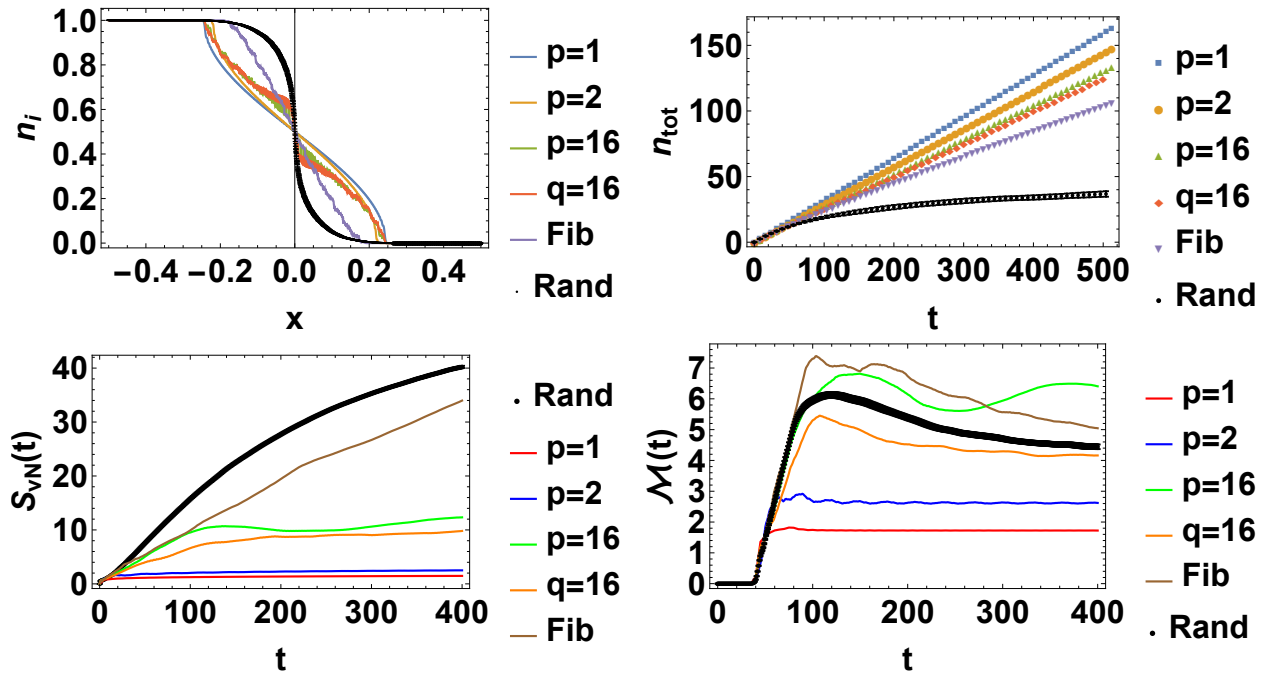


FIG. 2: (Colour Online) Top Left:- Plot showing $n_i = \langle c_i^\dagger c_i \rangle$ at time $T = 500$ in units of J^{-1} . Top right:- Plot showing $n_{tot} = \sum_{i=L/2+1}^L \langle c_i^\dagger c_i \rangle$ vs T for the different configurations. Bottom Left:- Plot of Von Neumann Entropy S_{vN} as function of time for a subsystem of size $M = L/2$. L is chosen to be 2048 for all cases except Fibonacci where it is 2584. The site A is chosen at $i = L/2 + 1$. Bottom Right:- Plot of Mutual Information vs Time for subsystem α spanning sites $i = L/2 + 1$ to $i = L/2 + 40$ and β spanning sites $i = L/2 + 41$ to $i = L/2 + 80$. The width of the line denotes the errorbars in the Random cases. See text for details.

sequences refer supplementary material.

The bottom left panel of Fig. 2 however paint a different picture. The Entanglement Entropy between two halves of the system separated by $i = L/2$ shows an exact opposite behaviour to the local $\langle c_i^\dagger c_i \rangle$ correlators. This means higher the inhomogeneity in the system the larger the entanglement. The bottom right panel shows information leakage between two subsystems in the region $i > L/2$. Even there the disordered case shows a very high leakage of information, but it's lower than the Fibonacci potential case and some periodic potential cases. This is an extremely counter intuitive result as even though a much lower number of particles enter the right half of the system as we break TS, the EE is actually higher! In the case of both global and local quenches, the quasiparticle picture states that entanglement is generated when a quasiparticle originating from the surroundings enters the subsystem, hence the higher the number of quasiparticles entering, higher the entropy. But here, clearly, the situation is different. So a closer look is needed to understand this phenomenon.

Entanglement Entropy between a system and a surroundings is generated both when particles tunnel in as well as out of the system. When the potential landscape is not translation invariant scattering events occur which cause movement of particle density flux in

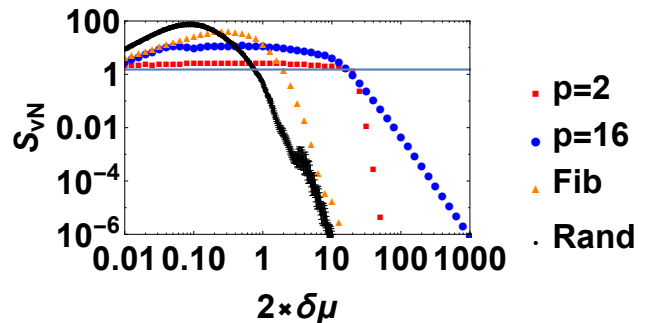


FIG. 3: (Colour online) Plot showing Von Neumann entropy vs strength of inhomogeneity denoted by $\delta\mu$ at $T = 500$ for different representative cases. The subsystem is of length $M = L/2$, and the position of A is at $i = L/2 + 21$ and hence $M = L/2 - 20$. The line denotes the Entanglement for $\delta\mu = 0$. The rest of the parameters are same as Fig 2. See text for details.

both directions. This situation occurs for all types of quenches. However, the difference is, for the domain wall initial state, in the case of $\delta\mu = 0$ system, there is only one travelling wavefront which causes transportation of particles. This is contrary to the case of global quench where a wavefront emanates from each lattice site. The number of wavefronts reaching and consequently

leaving the subsystem defines the amount of information transferred to the system under consideration. However on breaking of the translation symmetry, points in the potential landscape from where particles get scattered is created. These scattering events generate new travelling wavefronts in both directions. In case of the domain wall initial state, due to presence of only one travelling wavefront otherwise, this causes a sharp rise in entanglement and information propagation while it is not relevant in global quenches.

However, number density of particles still has a role to play in entropy as shown by the information leakage plot in the bottom right panel. The farther we go from $i = L/2$, the lower the number density falls for localized systems. Hence in the disordered case even if there is a high information leakage, it is lower than some other cases in which the density of particles in the subsystem β is higher. This effect is expected since if a wavefront does not reach a particular region of the system (i.e. we are looking at a set of sites beyond the localization length of the system), it cannot convey information. Hence, the number density of particles crossing a subsystem i.e. the position and structure of wavefront is also relevant in Entanglement. This reiterates intuitive notion of Entanglement of quasiparticles carrying entropy. In case of a global quench, for a translationally invariant problem, $O(N)$ number of wavefronts are created at $T = 0$ and they travel ballistically to all parts of the system. Hence the much slower moving wavefronts containing lower particle density due to scattering events play little to no role in Entanglement and the results can be understood from the intuitive quasiparticle picture. For a local quench, since the number density of the travelling wavefront is small (intensive), the effect of increase of wavefronts created with an even lower number density does not increase the entanglement. However in an inhomogeneous quench (or a domain-wall initial state) the presence of only one travelling wavefront in the TS system and the density gradient aiding a flow of particle current allows the wavefronts created due to scattering for TS broken systems to reach $x > 0$ subsystems. Thus just the intuitive picture of Entanglement being proportional to the number of particles in the system becomes insufficient. While the scattered wavefronts show slower than ballistic propagation, they carry a significant particle density and are large enough in number to result in a much higher rate of information leakage compared to TS systems. Thus for domain wall initial states scattering events play a very significant role in enhancing information leakage. And for a small disorder the localization length and the particle density in the $i > L/2$ part of the system becomes large enough to facilitate substantially faster information leakage from the left half of the system to the right. In the next paragraph, we discuss what happens when the strength of $\delta\mu$ is increased. For further interesting aspects of entanglement in inhomogeneous quench, refer

the supplementary material.

Fig. 3 shows the behaviour of Entanglement Entropy for a representative time $T = 500$ (which is within thermodynamic limit) for different strength of $\delta\mu$. The subsystem AB is chosen from $i = L/2 + 20$ to $i = L$. As expected, in random disorder and other symmetry breaking potentials the entanglement drops off as a power law with $\delta\mu$. It is also important to note different potentials follow a different power law which occurs due to the nature of scattering events encountered. It is to be expected correlated and uncorrelated scatterings result in different behaviour. Even in correlated scattering the scattering from a periodic potential is different from a quasi-periodic one. The supplementary material has a short discussion about the power laws seen and a peculiar behaviour of random disorder at high $\delta\mu$.

IV. DISCUSSION

In this work we have shown and explained that breaking of Translation Symmetry in a 1D free fermion system under an inhomogeneous quench has an effect of increase of Information leakage and Entanglement, within a limit of strength of the potential. The fascinating aspect of this result is, in 1D even a small disorder causes onset of localization but localization aids Entanglement in spite of resulting in less particles being involved in the information transport. We have explained this phenomenon from the wavefront picture generated from scattering of particles and via a physical understanding of how information propagates between two systems. We have also discussed why this effect is so prominent in inhomogeneous quench while is non-existent in global and local quenches. Finally we have numerically calculated the strength of the potential required to overturn this effect to get the more expected phenomenon. This also gives us an idea of the length-scale and time-scale in which this phenomenon occurs which we describe below.

For weak disorder, large localization lengths result in very high values of EE. One needs to wait for a time of $t \sim e^{200}$ for half-chain EE due to a TS system match the half-chain EE in disordered system having $\delta\mu = 0.1$.³³ Another way to look at it is, for weak disorder, upto a critical length of the subsystem dependent on potential type and strength, EE is higher for TS broken case than the TS case. And this length can actually be exponentially larger than the localization length of the system. It is explained in the supplementary material, that for a subsystem of size M , for TS system, EE goes as $0.3374 \log M + 1.4052$ for even M and $0.3346 \log M + 0.72613$ for odd M . So for $\delta\mu = 0.1$, one can choose a system size as large as $e^{100} = 10^{43}$ for even M and even then the entropy due to disorder will give a higher value in spite of localization to a length of around 100. For odd M the size can be even

larger. Thus our result is essentially valid for even thermodynamically large systems for weak disorder strength. If one chose the subsystem entirely away from the localization length however, this effect will not be observed. However for most practical cases we choose one end of the subsystem A at $i = L/2 + 1$ because at $T = 0$ we glued two systems together at $i = L/2$ and we want to compute the EE between the two systems. The domain wall initial state then ensures along with weak disorder that the localization length will go beyond that site.

This work serves to show the technique of applying inhomogeneity to trap quantum information in a system of qubits needs careful consideration of the initial states and the strength of the potential. For domain-wall initial states a small disorder will enhance leakage of information and fail the purpose. So this study is important in the field of quantum information.

While the numerical results are exact, there is non-

rigorous analytic framework to treat inhomogeneous quench in the symmetry broken systems. A proper theoretical handle to explain the various power laws and other results shown in this work is an open question. Effect of non zero interaction term on the results is an important avenue to extend the results of this problem to increase its application in real world systems. Validity of the results in higher dimensions and other kinds of defects e.e. vortex defects can be studied as well.

Acknowledgement

RG thanks Prof. A. Sen for discussions and introducing him to problems with domain wall initial states, Prof. K. Sengupta and B. Mukherjee for discussions, and CSIR SPM fellowship for financial support.

-
- ¹ Vincenzo Alba and Fabian Heidrich-Meisner. Entanglement spreading after a geometric quench in quantum spin chains. *Phys. Rev. B*, 90:075144, Aug 2014.
 - ² Jorn Mossel, Guillaume Palacios, and Jean-Sébastien Caux. Geometric quenches in quantum integrable systems. *Journal of Statistical Mechanics: Theory and Experiment*, 2010(09):L09001, sep 2010.
 - ³ T. Antal, Z. Rácz, A. Rákos, and G. M. Schütz. Transport in the XX chain at zero temperature: Emergence of flat magnetization profiles. *Phys. Rev. E*, 59:4912–4918, May 1999.
 - ⁴ T. Antal, P. L. Krapivsky, and A. Rákos. Logarithmic current fluctuations in nonequilibrium quantum spin chains. *Phys. Rev. E*, 78:061115, Dec 2008.
 - ⁵ Viktor Eisler and Zoltán Rácz. Full counting statistics in a propagating quantum front and random matrix spectra. *Phys. Rev. Lett.*, 110:060602, Feb 2013.
 - ⁶ Jarrett Lancaster and Aditi Mitra. Quantum quenches in an xxz spin chain from a spatially inhomogeneous initial state. *Phys. Rev. E*, 81:061134, Jun 2010.
 - ⁷ Thiago Sabetta and Grégoire Misguich. Nonequilibrium steady states in the quantum xxz spin chain. *Phys. Rev. B*, 88:245114, Dec 2013.
 - ⁸ Mrton Kormos. Inhomogeneous quenches in the transverse field Ising chain: scaling and front dynamics. *SciPost Phys.*, 3:020, 2017.
 - ⁹ Márton Kormos, Cătălin Pașcu Moca, and Gergely Zaránd. Semiclassical theory of front propagation and front equilibration following an inhomogeneous quantum quench. *Phys. Rev. E*, 98:032105, Sep 2018.
 - ¹⁰ Katja Klobas, Marko Medenjak, and Tomaž Prosen. Exactly solvable deterministic lattice model of crossover between ballistic and diffusive transport. *Journal of Statistical Mechanics: Theory and Experiment*, 2018(12):123202, dec 2018.
 - ¹¹ Jacopo Viti, Jean-Marie Stéphan, Jérôme Dubail, and Masudul Haque. Inhomogeneous quenches in a free fermionic chain: Exact results. *EPL (Europhysics Letters)*, 115(4):40011, Aug 2016.
 - ¹² Tibor Rakovszky, C. W. von Keyserlingk, and Frank Pollmann. Entanglement growth after inhomogeneous quenches. *Phys. Rev. B*, 100:125139, Sep 2019.
 - ¹³ Jean-Paul Allouche and Jeffrey Shallit. *Automatic sequences. Theory, applications, generalizations*. Cambridge: Cambridge University Press, 2003.
 - ¹⁴ Wai fong Chuan. Fibonacci words. *Fibonacci Q.*, 30(1):68–76, 1992.
 - ¹⁵ Wai-fong Chuan. *Subwords of the Golden Sequence and the Fibonacci Words*, pages 73–84. Springer Netherlands, Dordrecht, 1996.
 - ¹⁶ Ingo Peschel. Calculation of reduced density matrices from correlation functions. *Journal of Physics A: Mathematical and General*, 36(14):L205–L208, mar 2003.
 - ¹⁷ H Casini and M Huerta. Entanglement entropy in free quantum field theory. *Journal of Physics A: Mathematical and Theoretical*, 42(50):504007, dec 2009.
 - ¹⁸ Siew-Ann Cheong and Christopher L. Henley. Many-body density matrices for free fermions. *Phys. Rev. B*, 69:075111, Feb 2004.
 - ¹⁹ Siew-Ann Cheong and Christopher L. Henley. Operator-based truncation scheme based on the many-body fermion density matrix. *Phys. Rev. B*, 69:075112, Feb 2004.
 - ²⁰ Pasquale Calabrese and John Cardy. Evolution of entanglement entropy in one-dimensional systems. *Journal of Statistical Mechanics: Theory and Experiment*, 2005(04):P04010, apr 2005.
 - ²¹ Pasquale Calabrese and John Cardy. Time dependence of correlation functions following a quantum quench. *Phys. Rev. Lett.*, 96:136801, Apr 2006.
 - ²² Vincenzo Alba, Pasquale Calabrese, and Erik Tonni. Entanglement spectrum degeneracy and the cardy formula in 1+1 dimensional conformal field theories. *Journal of Physics A: Mathematical and Theoretical*, 51(2):024001, dec 2017.
 - ²³ Pasquale Calabrese and John Cardy. Entanglement and correlation functions following a local quench: a conformal field theory approach. *Journal of Statistical Mechanics: Theory and Experiment*, 2007(10):P10004–P10004, oct 2007.

- 2007.
- ²⁴ Dominique Gobert, Corinna Kollath, Ulrich Schollwöck, and Gunter Schütz. Real-time dynamics in spin- $\frac{1}{2}$ chains with adaptive time-dependent density matrix renormalization group. *Phys. Rev. E*, 71:036102, Mar 2005.
- ²⁵ Viktor Eisler and Ingo Peschel. Evolution of entanglement after a local quench. *Journal of Statistical Mechanics: Theory and Experiment*, 2007(06):P06005–P06005, jun 2007.
- ²⁶ Pasquale Calabrese and John Cardy. Quantum quenches in 1+1 dimensional conformal field theories. *Journal of Statistical Mechanics: Theory and Experiment*, 2016(6):064003, jun 2016.
- ²⁷ Elliott H. Lieb and Derek W. Robinson. *The Finite Group Velocity of Quantum Spin Systems*, pages 425–431. Springer Berlin Heidelberg, Berlin, Heidelberg, 2004.
- ²⁸ Jean-Paul Allouche and Jeffrey Shallit. The ubiquitous prouhet-thue-morse sequence. In C. Ding, T. Helleseth, and H. Niederreiter, editors, *Sequences and their Applications*, pages 1–16, London, 1999. Springer London.
- ²⁹ Jean-Paul Allouche and Laurence Maillard-Teyssier. Inconstancy of finite and infinite sequences. *Theoretical Computer Science*, 412(22):2268 – 2281, 2011.
- ³⁰ A. P Siebesma and L Pietronero. Multifractal properties of wave functions for one-dimensional systems with an incommensurate potential. *Europhysics Letters (EPL)*, 4(5):597–602, sep 1987.
- ³¹ Qian Niu and Franco Nori. Spectral splitting and wavefunction scaling in quasicrystalline and hierarchical structures. *Phys. Rev. B*, 42:10329–10341, Dec 1990.
- ³² Michele Modugno. Exponential localization in one-dimensional quasi-periodic optical lattices. *New Journal of Physics*, 11(3):033023, Mar 2009.
- ³³ In supplementary material we show a fit of the data for the half chain TS system to $0.476 + 0.167 \log(t)$, plugging the value of Entanglement Entropy due to the disorder as ~ 40 we get the required timescale

Supplementary Material

A. Calculation of $\langle c_m^\dagger(t)c_n(t) \rangle$

Since this is an integrable model, we can exploit the fact that all the information about the system is contained in the one particle sector of the Hamiltonian. We can thus reduce the $2^N \times 2^N$ problem to the $N \times N$ problem in theory, but in practice, if we were to work in the Schrödinger picture we would have to still deal with $\binom{N}{m}$ eigenfunctions for a m particle sector in a N site model which are constructed as Slater determinants of the 1-particle sector. But luckily we are not interested in wave functions here, and hence we can switch to the Heisenberg picture and deal with $N \times N$ matrices and find the required result. The entire procedure for this is as follows,

$$\begin{aligned} \mathcal{H} &= \mathbf{c}^\dagger \mathbf{C} \mathbf{c} \\ &= \mathbf{c}^\dagger U^\dagger U C U U^\dagger U \mathbf{c} \\ &= \mathbf{b}^\dagger \mathbf{B} \mathbf{b} \end{aligned}$$

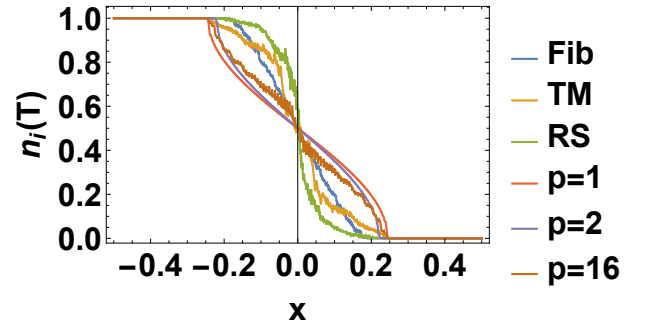


FIG. 4: (Colour online) Plot showing $n_i = \langle c_i^\dagger c_i \rangle (T)$ vs $x = (i - L/2)/L$ at $T = 500$ for various systems considered in the paper. Notice how, as we go towards chaotic sequences the wavefront gets localized near $x = 0$. Also notice the $p = 16$ case shows an interesting structure in n_i . This is due to the periodicity of lattice, where there is a smaller density of particles on every p^{th} site for $x > 0$ and vice-versa for $x < 0$, this effect is more prominent with increasing p , upto a value which is same as the p for maximum entropy.

where $\mathbf{B} = U C U^\dagger$ and $\mathbf{b}^\dagger = \mathbf{c}^\dagger U^\dagger$ or $b_i^\dagger = c_j^\dagger U_{ji}^\dagger = U_{ij}^* c_j^\dagger$ and $b_k = U_{kj} c_j$ where \mathbf{B} denotes the diagonalized matrix and \mathbf{b} denotes the diagonal basis. In this basis we know the Hamiltonian is $\mathcal{H} = -\sum_k E_k b_k^\dagger b_k (E_k = B_{kk})$, and hence ,

$$b_k(t) = b_k(0) e^{itE_k}, \quad b_k^\dagger(t) = b_k^\dagger(0) e^{-itE_k} \quad (7)$$

Using these expressions we can write the time dependent correlation matrix. Also we recall that $\mathbf{c} = U^{-1} \mathbf{b} = U^\dagger \mathbf{b}$ or $c_i = U_{ij}^\dagger b_j = b_j U_{ji}^*$. Using this and remembering that for the systems considered in this paper the U matrices are all real.

$$\begin{aligned} \langle c_m^\dagger(t) c_n(t) \rangle &= \sum_{k,l} U_{km} U_{ln} \langle b_k^\dagger(t) b_l(t) \rangle \quad (8) \\ &= \sum_{k,l} U_{km} U_{ln} e^{-iE_k t} e^{iE_l t} \langle b_k^\dagger(0) b_l(0) \rangle \\ &= \sum_{k,l,i,j} U_{km} U_{ln} U_{ki} U_{lj} e^{i(E_k t - E_l t)} \times \\ &\quad \langle c_i^\dagger(0) c_j(0) \rangle \end{aligned}$$

Using the known initial conditions $\langle c_i^\dagger(0) c_j(0) \rangle$ we can figure out the evolution .

B. Constant potentials

For periodic boundary conditions, if $\mu_p = \mu$ then, this system can be diagonalized in momentum space to give,

$$\mathcal{H} = -\sum_k (\cos(k) - \mu) b_k^\dagger b_k \quad (9)$$

where $k = \frac{2\pi n}{L}$ and $n = 0, 1, \dots, L-1$ is the momentum index of the system. Now using Heisenberg's equation of

motion, we can figure out the time evolution of b_k as,

$$\dot{b}_{k'} = -i[b_{k'}, \mathcal{H}] = i(\cos(k) - \mu)b_{k'} \quad (10)$$

which gives us,

$$b_k(t) = b_k(0)e^{i(\cos(k)-\mu)t}, \quad b_k^\dagger(t) = b_k^\dagger(0)e^{-i(\cos(k)-\mu)t} \quad (11)$$

Now our aim is to find $\langle c_m^\dagger c_n \rangle(t)$, which written in Heisenberg picture looks like $\langle c_m^\dagger(t)c_n(t) \rangle$. The set of steps to this is as follows,

$$\begin{aligned} c_n(t) &= \sum_k e^{ink} b_k(t) \\ &= e^{-i\mu t} \sum_k e^{ink} b_k(0) e^{it \cos(k)} \\ &= e^{-i\mu t} \sum_{k,j} e^{ink} e^{it \cos k} e^{-ikj} c_j(0) \\ &= e^{-i\mu t} \sum_{k,j} \sum_{\alpha=-\infty}^{\infty} e^{i[n-j]k} i^\alpha J_\alpha(t) e^{i\alpha k} c_j(0) \\ &= e^{-i\mu t} \sum_j i^{n-j} J_{n-j}(t) c_j(0) \end{aligned}$$

Hence,

$$\begin{aligned} \langle c_m^\dagger(t)c_n(t) \rangle &= \sum_{j,k} i^{n-j} (-i)^{m-k} J_{n-j}(t) J_{m-k}(t) \\ &\times \langle c_k^\dagger(0)c_j(0) \rangle \end{aligned} \quad (12)$$

From the initial condition of the system,

$$\begin{aligned} \langle c_p^\dagger c_q \rangle &= \delta_{pq} \quad p \leq N/2 \\ &= 0 \quad \text{otherwise} \end{aligned} \quad (13)$$

after several straightforward but tedious lines of algebra using recursion relation of Bessel functions, we obtain a more tractable form which is as follows,

$$\begin{aligned} C_{mm}(t) &= \langle c_m^\dagger c_m(t) \rangle = \frac{1}{2} [1 - J_0^2(t)] - \sum_{l=1}^{m-1} J_l^2(t) \\ C_{mn}^{m \neq n}(t) &= \frac{i^{n-m} t}{2(m-n)} [J_{m-1}(t) J_n(t) - J_{n-1}(t) J_m(t)] \end{aligned}$$

For open boundary conditions, one can also find the eigenvalues as,

$$\mathcal{H} = - \sum_k (\cos(k) - \mu) b_k^\dagger b_k$$

where $k = \frac{\pi n}{L+1}$ and $n = 0, 1, \dots, L-1$. However, it is easier to follow the numerical prescription given in Eq. 8 to find out the time evolution. For a sanity check, in Fig. 5 we show the comparison of the results in the periodic BC and open BC. As expected for a finite subsystem size if we are in the thermodynamic limit, the results show no difference. But on breaking the limit, the wavefront

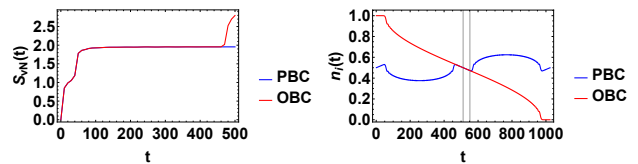


FIG. 5: (Colour online) Left:- Plot of S_{vN} vs t for a subsystem of size $M = 40$ for a system with Periodic Boundary Conditions (PBC) compared to one with Open Boundary Conditions (OBC) showing exact same results till thermodynamic limit. Right:- Plot of $n_i = \langle c_i^\dagger c_i \rangle$ vs i at $T = 460$ in units of J^{-1} , for PBC and OBC conditions, showing the region where they overlap. The thermodynamic limit for the $m = 40$ subsystem would be broken at $t = 472$ considering ballistic propagation. It is seen at $t = 460$ the overlap is still perfect in the region of the subsystem denoted by the two gridlines, and hence either analysis gives equivalent results.

reflected from the boundary walls start interfering with the wavefront going towards the walls and the distribution for PBC and OBC show a difference. Since the work mostly deals with systems in thermodynamic limit, this feature is not relevant in our work. We now show the numerical results obtained for the system described in this section. Since we have derived exact analytical formulas for the correlation function, we would be using those expressions to calculate entanglement measures in this system. Fig. 6 shows the growth of Von Neumann entropy with time for different subsystem sizes denoted by M . As expected,¹⁸ the entanglement entropy at large times is higher for higher subsystem sizes. Due to the fact that the correlation functions at large times equal that to the correlations calculated in the ground state of this Hamiltonian, it can be shown the entanglement goes as $\log M$.¹⁹ In fact it was shown in the reference that the data can be fitted exactly to $0.3374 \log M + 1.4052$ for even M and $0.3346 \log M + 0.72613$ for odd M

A peculiar feature of this figure however is that the EE vs T shows two sharp increases, one at $t = 0$ and another at $t = T_2$ before it saturates. This is unlike the case of global quenches in free systems where the initial state can be written in terms of pairs of quasiparticles,²⁰⁻²² where they have shown via CFT arguments that there would be a linear increase in entropy at first after which it tends to saturate, and there is no second point of increase. Additionally, the increase till $t = T_2$ can be nicely fit in a $\log(t)$ behaviour. This is reminiscent of the behaviour of entanglement entropy dynamics in two halves after a local quench as predicted by Calabrese Cardy²³, and was presented in^{24,25}. Thus this particular quench can be described as a quench in between a global and a local quench and has been well known in literature as an inhomogeneous quench,²⁶ or a geometrical quench¹. The argument is that, even if the initial state considered here has an extensively different energy than the ground state of the system, the Pauli exclusion principle prevents

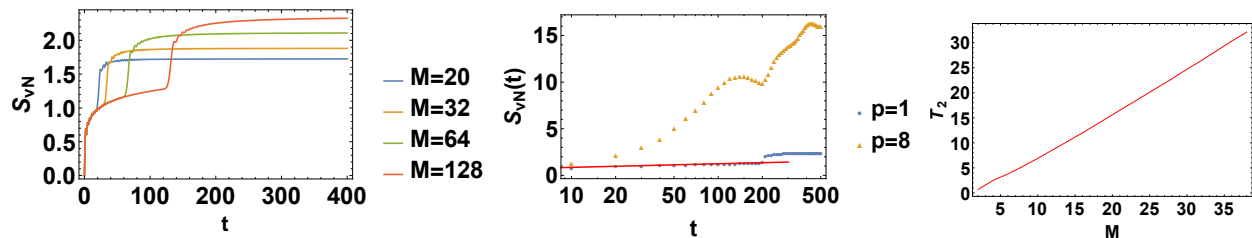


FIG. 6: Left Panel:- Plot showing growth of von Neumann entropy with time for a subsystem of M sites to the right of $L/2$ with time. Middle:- Plot showing the fit of $\log t$ with the data for a subsystem of size $M = 200$. p denotes the periodicity of the potential. Hence $p = 1$ denotes the constant μ case. The red line shows the fit of $S_{vN} = 0.476 - 0.167 \log(t)$ with the data. Right:- The figure shows a comparison of the point of time (T_2) at which the Entanglement entropy shows a sudden jump for different subsystem sizes M . See text for details

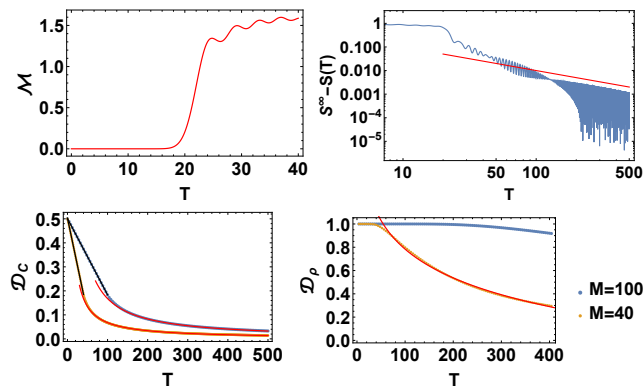


FIG. 7: (Colour online) Top Left:- Plot showing growth of Mutual information \mathcal{M} with time for a subsystem of M sites to the right of $N/2$ and a subsystem of M sites to the right of $N/2 + M$ with time. M is chosen to be 20. Top Right:- Plot showing approach of EE to the diagonal ensemble of a subsystem of size $M = 100$, showing presence of two distinct timescales. For $t \gg T_2$ it is clear the entanglement goes to the diagonal value as t^{-1} . Bottom Left:- Plot showing the evolution of the trace distance between the diagonal ensemble correlation matrix and $C_{ij}(T)$ for two different system sizes. The black line is the fit for the section of data at $t < T_2$ as $S_{vN} \propto t$. The red line is the fit of the data at times $t > T_2$ as $S_{vN} \propto 1/t^{1.017}$ for $M = 100$ and $S_{vN} \propto 1/t^{0.99}$ for $M = 40$. Bottom Right:- Plot showing the evolution of the trace distance between the diagonal ensemble reduced density matrix and $\rho(t)$ for the same two system sizes. The red line shows the fit of the data to $\log(t)$. See text for details

quasiparticles/wavefronts to be created in an extensive manner throughout the system at $t = 0$. The important thing to note is that the transport of particles and the local correlations are ballistic (as shown by fig) but the non local correlations travel in slower than that as presented by the trace distance of the density matrix and the entanglement evolution. In fact one can see there are two distinct time scales of the system and until the wave reaches the end of the subsystem, non local correlators evolve exponentially slowly. This can again be attributed to the fact that a quench from such an initial state behaves more like a local quench than a

global quench, as there is only one developing wavefront. However note that, in local quenches where only an intensive number of quasiparticles are pumped into the subsystem, and hence the initial $\log(t)$ behaviour will be replaced by a decrease once the particle has left the subsystem or a saturation value as the quasiparticle goes deeper inside the subsystem. Here as long as particles are being pumped into the subsystem from on defect site the $\log(t)$ behaviour will continue, that is unless the particles see a ‘wall’. Several things can qualify as a ‘wall’, it can be the end of a finite sized subsystem under consideration, labeled by B , where the EE shows another jump at $T = T_2$, or it can be the fact the particles get reflected (transmitted) from a finite sized system with open (periodic) boundary conditions and reach $x = 0$ which was the position of A . In either of these cases EE shows a jump since a wavefront entering or leaving a system generates entanglement with the surrounding. How EE approaches equilibrium for a finite sized translationally invariant system after multiple reflections from the boundary has been shown in Alba¹. We extend those results later and show how this particular feature of growth of entanglement when a wavefront crosses the domain wall extends to translational symmetry broken system and generates interesting results. Our findings are completely consistent with the light cone spreading of correlation function and the Lieb-Robinson bound for the group velocity of quasiparticles.²⁷.

We describe below how one can qualitatively understand the second jump at $t = T_2$. Since initially, all correlations to the right of $x = 0$ point was 0, where x is the site position so there could not be any Entanglement between any subsystem and the surroundings. As soon as we switch on the Hamiltonian, correlations between neighbouring sites start developing near the origin and spread towards left and right with a group velocity v . One can think of this as carried by two wavefronts (consisting of particles) travelling left and right from the domain wall at the origin entangling the subsystem with the left half of the lattice. Hence there is an initial rise in entanglement.

With time the wavefront travelling to the right reaches the end point of the subsystem and then crosses over to that part of the system which was not accessible initially. This allows correlations to form between the part which was inaccessible earlier and the subsystem under consideration. It is at this moment the second jump in entanglement is observed. This theory is further strengthened by the plot of T_2 vs M where T_2 is the time in which the second jump starts and M is the subsystem size, plotted in the right panel of figure 1. It shows a linear increase with subsystem size. The tolerance level for calculation of T_2 was chosen to be 10^{-4} . The time T_2 exactly matches with the time at which Mutual information between this subsystem and a subsystem of 20 sites chosen just to the right starts increasing from a 0 value which is shown in the top left panel of Fig. 6. This also shows a nice picture of how Entanglement is generated between two systems as particles go from one system to another.

Thus, there is two timescales in this problem, before and after $t = T_2$. The rise of entanglement after $t = T_2$ does not follow a $\log(t)$ behaviour here as can be seen from the middle panel of Fig. 6. In the Logarithmic scale the rise is almost vertical and then it slows down drastically while going to its diagonal ensemble value in a ballistic fashion. In fact after $t = T_2$ the EE goes to its diagonal ensemble value in a ballistic manner as t^{-1} . This behaviour of EE for a finite subsystem is more reminiscent of the EE dynamics of a system under a global quench than a local quench. In the local quench, it has been shown once the intensive number of quasiparticles leave the subsystem, the entanglement entropy asymptotically decreases to the ground state value. To be noted, there the initial state of choice there was a state whose EE was not zero but extremely close to the ground state values. But here, we started from a state whose EE was 0, extensively away from the ground state, and as there is a continuous pump of particles through the subsystem such a decrease is not observed but instead it becomes steady at a finite value. The intriguing thing is however is, even in this case the diagonal ensemble EE exactly matches the EE of the ground state of the Hamiltonian and thus it is not an extensive quantity unlike what is expected of a global quench, within the thermodynamic limit. This is due to the fact, the correlation functions, at $T \rightarrow \infty$ have an absolute value same as the ground state correlators with a position-dependent phase in the off-diagonal terms. Thus state goes to an eigenstate of the Hamiltonian which is not the ground state.³ This happens mainly due to the integrable nature of the system. However, mathematically the Eigenvalues of C_{mn} , compared to the eigenvalues of the correlation matrix of the ground state of the system, has no difference, as these two Toeplitz matrices are similar matrices. In the wave picture, we believe that when we choose a finite sized subsystem AB , the wave from the domain wall at

$x = 0$ would propagate through the subsystem, but on seeing site B it breaks up into a reflected and transmitted wave. The reflected and the incoming wave undergo interference to set up standing waves which in turn are eigenfunctions of the Hamiltonian, and thus the DE behaves as it does. This anomalous behaviour carries over to other non local correlators like the trace distance measure between ρ_D and $\rho(t)$ which we plot in the bottom right panel of Fig 6. In the bottom left panel of Fig 6, we plot the trace distance between just the local correlation functions. ($\mathcal{D}_C = C^\infty - C(t)$). As one can see for $t < T_2$, it goes towards the DE in an almost linear manner because it can be fit almost perfectly to T behaviour. For $t > T_2$ the behaviour changes to $\sim t^{-1}$ which again points out $t = T_2$ is a special point. It is worthy to note that even though the entanglement falls off as t^{-1} for $t > T_2$, the trace distance of the density matrix \mathcal{D}_ρ shows $\log(t)$ sort of a fall. For $t < T_2$ the density matrix goes exponentially slowly towards the diagonal ensemble. Hence we state that for this system the local correlations reach towards the DE faster than non local quantities. Physically, when the wavefront travels through the subsystem, until $t = T_2$ it does not see the right boundary or B . At this time the correlators go towards the DE value of the subsystem linearly and entanglement grows as $\log(t)$. Once it reaches the point B at $t = T_2$, immediately there is a reflected wavefront which interferes with the incoming wave. As soon as this happens the scaling law changes, and the local correlators as well as EE are seen to go to their DE values as T^{-1} and the Trace distance of the density matrix as $\log(t)$.

C. Periodic Potentials

In this section we will discuss in details the first type of Periodic potential described in the main text. We choose $\mu_m = \mu_0 + (-1)^{\sum_{n=1}^L \delta_{m,np}} \delta\mu$. As one can see such systems are not translationally invariant but the simplest case of $p = 2$ still has sufficient symmetry to attempt analytical diagonalization. We can see the system is a bipartite lattice in which the Hamiltonian can be broken up into 2×2 blocks in the momentum space as,

$$\mathcal{H} = \begin{pmatrix} c_k^\dagger & d_k^\dagger \end{pmatrix} \begin{pmatrix} \mu_1 & -\cos(k) \\ -\cos(k) & \mu_2 \end{pmatrix} \begin{pmatrix} c_k \\ d_k \end{pmatrix}$$

where $c_k[d_k]$ are the annihilation operators for the odd[even] lattice sites. Subsequent diagonalization of the 2×2 blocks yield,

$$E_k^\pm = \frac{1}{2} [(\mu_1 + \mu_2) \pm \sqrt{(\mu_1 - \mu_2)^2 - \cos(k)}]$$

Using this expression, one can attempt to try and solve for $c_m(t)$ in terms of $c_p(0)$ and $d_q(0)$ to get,

$$\begin{aligned}
c_m(T) = \frac{1}{L} \sum_k e^{imk} [\beta_-(k) e^{-iE_k^+ T} (\alpha_+(k) \sum_p c_p(0) e^{-ikp} + \beta_+(k) \sum_q d_q(0) e^{-ikq}) \\
- \beta_+(k) e^{-iE_k^- T} (\alpha_-(k) \sum_p c_p(0) e^{-ikp} + \sum_q \beta_-(k) d_q(0) e^{-ikq})] \quad (14)
\end{aligned}$$

where $\beta_{\pm} = \frac{\mu_1 - E_k^{\pm}}{\sqrt{(\mu_1 - E_k^{\pm})^2 + (\cos k)^2}}$ and $\alpha_{\pm} = \frac{\cos(k)}{\sqrt{(\mu_1 - E_k^{\pm})^2 + (\cos k)^2}}$ are found from the eigenvectors of the block. However we see that this cannot be simplified easily into closed form expressions, so it is easier to use the numerical prescription to handle such systems.

Fig 8 shows the eigenvalue spectrum as well as occupation density at each site of the system of the ground state wavefunction. The eigenspectrum shows $p - 1$ gaps in it where p is the periodicity of the system. The occupation density throws up a more interesting feature, showing increasing inhomogeneity as we increase the periodicity further. This is in line with the data of Entanglement we got in our paper, as an increase of inhomogeneity means more scattering events which in turn raises the entropy if the subsystem is chosen in a particular manner as discussed.

In the figure 9 given below one spatially varies the chemical potential periodically, between two values of $\mu + \delta\mu$ and $\mu - \delta\mu$ where we have taken $\mu = 0.1$ and $\delta\mu = 0.1$ in units of J^{-1} . We consider four periods, $p = 2, 4, 8, 16$ which is well within the small period region where EE increases as we increase the period. A comparison with the translationally invariant problem immediately shows a higher entanglement than in that case.

There are several features in the graph which is worthy of notice. The first thing that strikes is the fact the wavy nature of the $\mu = 0$ EE shows a change. As we go to higher periods it seems the time period of the wave increases. This is because the problem in this limit does not solve to yield a simple sum of Bessel functions. It will be interesting if one is able to calculate an analytical expression of the functions involved in these cases.

Secondly in each of the figures of 9 there are four subsystem sizes, $M = 20, 40, 80$ and $M = L/2 = 1024$. All the time scales considered are within thermodynamic limit and one sees that for $p = 2$, the EE for the smaller subsystem sizes show a much stronger jump at $T = T_2$ from the large subsystem limit than when we go to $p = 4, 8, 16$. Thus as we introduce more gaps in the spectrum the jump at $T = T_2$ becomes a lot less pronounced. The reason for this is as we break the translation symmetry more, the wavefront encounters

a higher amount of scattering. And as we discussed in the main body of our work the higher number of wavefronts generated via scattering events crossing the subsystem play a very important role in information transfer in this system. This causes the entanglement to increase fast enough to wash out the sudden jump at $T = T_2$ which involves a lower number such events. However, as we shall see in the next sections, scattering affects the number of particles which would be present in $x > 0$ part of the system, and if there are too few such particles present and the wave cannot travel at all, then as expected Entanglement Entropy would be really small.

Above in left panel Fig. 10, we show the behaviour of entanglement entropy vs the period of modulation of the on site chemical potential μ for a fixed time chosen to be equal to the time just before which the thermodynamic limit of $\mu = 0$ system breaks down. This serves just to fix a time for which we can do the comparison, any time within the thermodynamic limit of this system gives equivalent results. Apart from the usual rise initially as we increase the period and the fall at very high periods where the system almost reaches a constant potential, we see several peaks and troughs which are surprisingly robust with system size. (The peaks appear for almost the same p/L). This is a surprising result which to the best of the knowledge of the author has not been discussed in literature. The five peaks appear at $p/L \sim 1/2, 1/4, 1/6, 1/8, 1/10$ suggesting these particular configurations have special symmetry that favours higher entropy. By the nature of the graph, one can also state that if the system size is made larger, more peaks will appear at $p/L = 1/12, 1/14, \dots$. One can see these values of p/L result in the site at the domain wall having a different μ to the ones surrounding it. To analyze what happens in these cases, we plot n_i vs i for several values of p in the right panel of 10, a few of which show the peaks and others don't. It can easily be seen the rise in entanglement can be correlated to the fact, for certain specific values of p/L particles start accumulating near $i = L/2$ or $x = 0$. This results in an increased number of wavefronts crossing the domain wall at $x = 0$ which causes the rise in entropy. It can be shown the further away the accumulation of particle is from the centre if at all there is accumulation, the lower the entropy is, hence $p = 400$ i.e. $p/L = 0.39$ shows a significantly lower value of entropy.

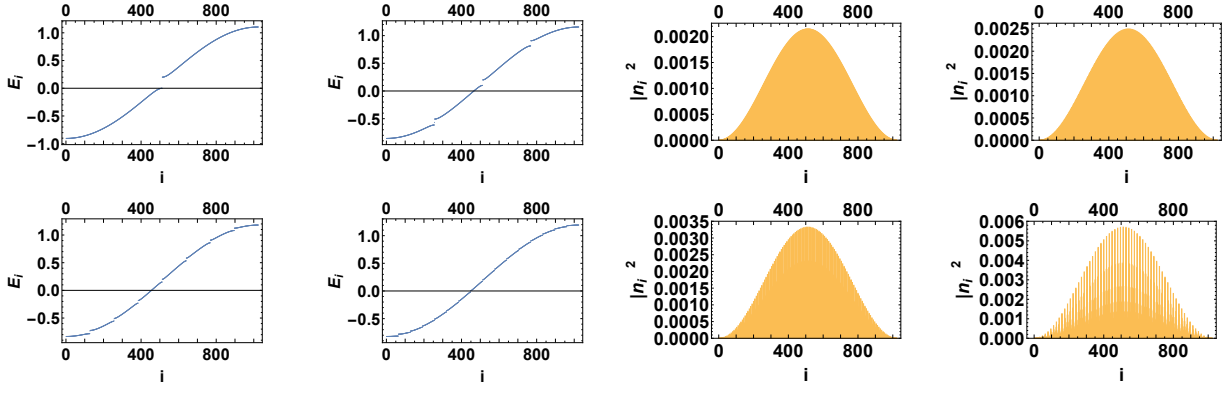


FIG. 8: Left:- The 4 panel figure in the left shows the eigenvalue spectrum of a system with periodic on-site potential. Starting from top left and going clockwise the periods are 2, 4, 8, 16. Right:- Plot of $|n_i|^2 = |\langle c_i^\dagger c_i \rangle|^2$ vs site i for the lowest energy eigenvector in each case of the left panel. See text for details

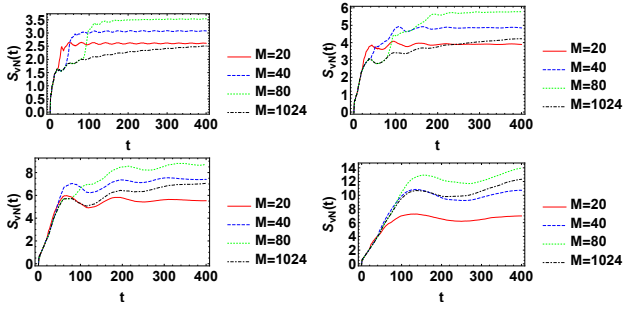


FIG. 9: Plot of S_{vN} vs t (in units of J^{-1}) for μ modulated periodically in space with a period (a) $p = 2$, (b) $p = 4$, (c) $p = 8$, (d) $p = 16$ for $\mu = 0.1$ and $\delta\mu = 0.1$ respectively. See text for details.

D. Automatic Sequence Potentials

1. Thue Morse sequence

Thue Morse sequence or more formally, Prohuet-Thue-Morse sequence²⁸ is another automatic sequence defined on the set of alphabets $\{0, 1\}$. There are several equivalent definitions for this sequence, here we state the most commonly used one. If T_n is the n^{th} word of the Thue Morse sequence and T_n^i is i^{th} letter(digit) in the word, then,¹³

$$T_n^i = s_2(i) \text{ mod } 2 \quad (15)$$

where $s_2(i)$ is the sum of binary digits of the decimal number i . The length of the n^{th} word is given by 2^n .

The first few words in the sequence are,

$$\begin{aligned} T_0 &= 0 \\ T_1 &= 01 \\ T_2 &= 0110 \\ T_3 &= 01101001 \\ T_4 &= 0110100110010110 \\ &\vdots \end{aligned}$$

A similar sequence can be created by taking 1's complement of T_n and it can be shown to have same properties as the original TM sequence. Similar to the case of Fibonacci words, we generate the on site potential using,

$$\begin{aligned} \mu_i &= \mu - \delta\mu, & T_L^i &= 0 \\ \mu_i &= \mu + \delta\mu, & T_L^i &= 1 \end{aligned} \quad (16)$$

The Thue Morse sequence is said to exist at the margin between quasi periodicity and chaos. This feature will be important for our analysis later.

2. Rudin Shapiro Sequence

Formally the Golay-Rudin-Shapiro sequence is another automatic sequence defined on the set of alphabets $\{0, 1\}$. If R_n is a word sequence of length n , then the i^{th} letter is given by the parity of the number of 11 (including overlaps) occurring in the binary representation of the number i ¹³. the length of the n^{th} word is the same as in the case for TM sequence, which is 2^n . Mathematically,

$$\begin{aligned} a_i &= \sum_{k=1}^i \epsilon_k \epsilon_{k+1} \\ R_n^i &= 1 + (-1)^{a_i} \end{aligned} \quad (17)$$

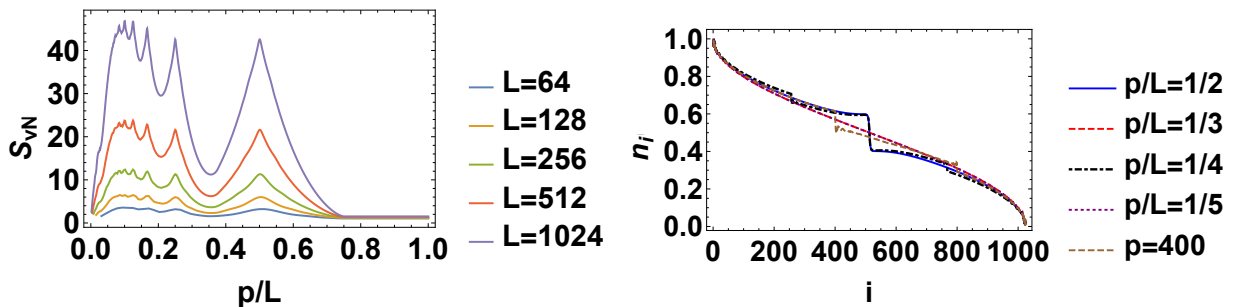


FIG. 10: (Colour online)Left:- Plot of S_{vN} of a subsystem of size $M = L/2$ at time $T = L/2$ in units of J^{-1} vs p/L where p is the period of the on site potential. Right:- Plot of $\langle c_i^\dagger c_i \rangle$ vs i at time $t = L/2$ in units of J^{-1} for different p showing how accumulation of particles occur at $L/2$ for certain specific periods. Note how the wavefront has just reached the end of the system at this moment in time, showing ballistic propagation. Refer text for details

where ϵ_k is the k^{th} digit in the binary representation of i . The first few terms of this sequence are,

$$\begin{aligned}
 R_1 &= 11 \\
 R_2 &= 1110 \\
 R_3 &= 11101101 \\
 R_4 &= 1110110111100010 \\
 &\vdots
 \end{aligned}$$

The potential is arranged in the same way as it was done for a TM sequence. It is interesting to note, that the potential arranged in Rudin Shapiro sequence shows the same characteristics in eigenvalues and eigenvectors as a completely chaotic potential. Indeed Allouche²⁹ defined a quantity called Inconstancy of a curve to characterize the nature of a sequence, showed that the RS sequence and the random sequence have exactly the same value of this parameter that can be used to characterize the sequence. The TM sequence also had a value which was close to the value obtained for the Random sequence, while the Periodic sequences had completely different values determined by the periodicity of the sequence considered. In Appendix B we discuss the one particle eigenvalues and eigenvectors than can be obtained from these types of potential landscapes. Fig. 11 shows the case for different automatic sequence potentials and the random potential. As expected, RS sequence and random sequence, shows a heavily localized one-particle ground state. For Fibonacci and TM sequence, we have a start of localization, but the number density vs site itself has a multifractal structure.³⁰ The self-similar structure also shows up in the eigenvalues in these cases as well, where the gaps are not periodic but follow a particular pattern. A good explanation of this structure is given in³¹. The difference in localization of eigenfunction at this strength of $\delta\mu$ corroborates our theory that correlated and uncorrelated scattering work differently, and maybe uncorrelated scattering events number is larger. This in turn fits nicely to the theory of higher Entanglement near the $x = 0$ point in our system considered.

The plot for the Von Neumann entropy vs Time for dif-

ferent subsystem sizes when the on-site potential is arranged in a Fibonacci sequence is given in the left panel of Fig 12. The system size is chosen to be $L = 2584$ for Fibonacci case and $L = 2048$ for Thue Morse case. The plot on the right panel of Fig 12 is when the potential is arranged in a Thue Morse Sequence. The data for $M = L/2$ is presented well within the time in which the system is in thermodynamic limit, i.e. within the time in which the wave does not reach the boundary of the system considered. Clearly, the jaggedness in the graph is greatly pronounced here due to complete lack of periodicity in the lattice. Furthermore the effect of scattering is clearly visible from the fact that EE grows even faster than in the periodic case, and the fact that jump at $T = T_2$ is even less pronounced. It also seems the effect of the jump at $T = T_2$ is more pronounced in the Thue-Morse case compared to the Fibonacci sequence along with the fact that the EE growth in this case is slower than the plot in the left panel. This feature is extremely counter-intuitive because Thue Morse sequence is considered a border between a quasi-periodicity and randomness, and as we will show in the next section a random sequence results in a much higher entropy with the same parameters.

Qualitatively, this feature can be attributed to the specific distribution of $n_i(T)$, the form of the quasiperiodic sequence allows. As shown in the left panel of Fig 13, the number density of particles present in the $x > 0$ part of the system is actually greater in the Fibonacci case than in the Thue Morse case. This suggests that there are less incidents of scattering in the Fibonacci case than the Thue Morse case. However, EE is actually controlled by the number of wavefronts crossing $x = 0$. In the middle panel of the same plot we show the first instance where $\langle c_i^\dagger c_i \rangle$ goes below a tolerance level of 10^{-2} which we have used to characterize the end of wavefront. This plot gives an idea of the position of the fastest particle in the system. As a sanity check we see for the TS particle is ballistic. We also see that the particle travels further in the case of TM sequence than Fibonacci sequence. Furthermore, a plot of n_i vs i for $T = 500$

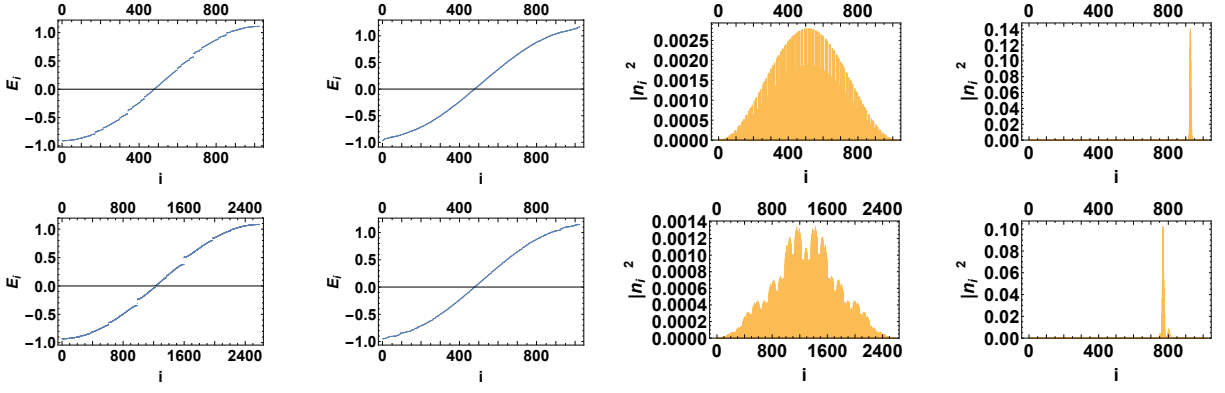


FIG. 11: Left:- The 4 panel figure in the left shows the eigenvalue spectrum of a system with automatic sequence or random on-site potential. Starting from top left and going clockwise the system's on-site potential are in TM, Random, Fibonacci and RS sequence. Right:- Plot of $|n_i|^2 = |\langle c_i^\dagger c_i \rangle|^2$ vs site i for the lowest energy eigenvector in each case of the left panel. See text for details.

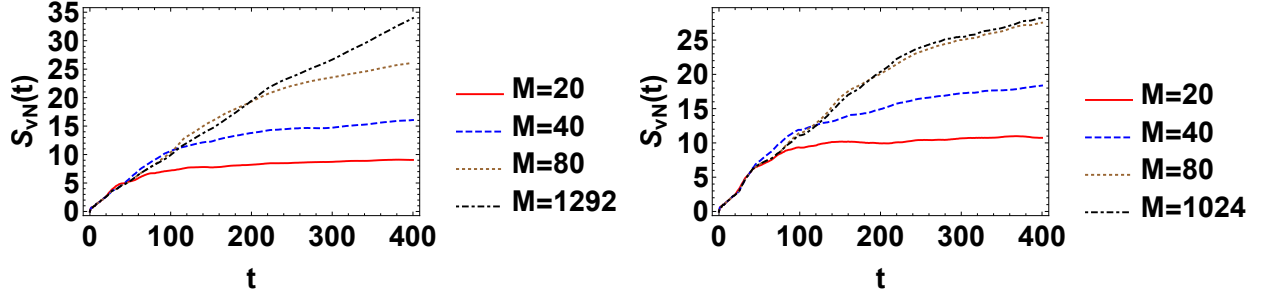


FIG. 12: Left:- Plot of Von Neumann entropy vs Time in a system where on site potential has values $\mu + \delta\mu$ and $\mu - \delta\mu$ arranged in a Fibonacci word sequence for different subsystem sizes. Right :- Plot of the same quantities but the on site potential is arranged in a Thue Morse sequence. The values are same as Fig 9. See text for details.

as shown in Fig. 14, where the x axis is scaled by the system length, shows the exact distribution, from where it is easy to see the spread in n_i for the TM case is much more pronounced than the Fibonacci sequence. An additional effect of this spread of n_i is reflected in the Mutual entropy between two subsystems described in the right panel of Fig. 13. TM sequence shows highest mutual entanglement between the two systems where as the other quasi-periodic and random sequences show a much lower value in spite of the EE being higher. (shown in the next section). To be noted, the same proximity to $x = 0$ resulting in a higher EE was a feature of the periodic case as well which we discussed in the previous section. Fig 15 shows the growth of Von Neumann entropy vs time for a system in which the on-site potential is arranged in a Rudin Shapiro sequence. It seems, scatterings under this type of potential are also larger in number to correlated scatterings of the Fibonacci sequence and thus the entanglement entropy grows faster to any of the cases discussed above. This is further seen in the fact that the jump at $T = T_2$ is even less pronounced than the previous cases in this sequence. A distribution of n_i at time $T = 500$ in Fig. 4, shows that it propagates exponentially slowly, a feature further corroborated by the extremely low value

of n_{tot} compared to the other distributions and almost matching the case of random distribution. Also the speed of the fastest particle significantly slows down after some time and the wave does not reach the end of the system for the system size considered here, even for large time. This essentially means these systems are going to a many body localized phase, while in quasi-periodic or periodic sequences the particles just slow down. Nevertheless this shows, that there are large number of scattering events happening near $x = 0$ which causes a large number of wavefronts to cross A of the subsystem causing in the rise in Entropy. However, as we shall see later, since an smaller number of particles cross $x = 0$ domain wall, if we see a very long time result for such systems, where particles are allowed to bounce back from the walls. This feature will be discussed in Sec. IV F.

E. Random Potential

For completeness, in this section we would discuss case in which the on-site potential is arranged as $\mu + \delta\mu$ and $\mu - \delta\mu$ distributed randomly throughout the lattice. Fig. 16 shows the case when the on-site potential is arranged

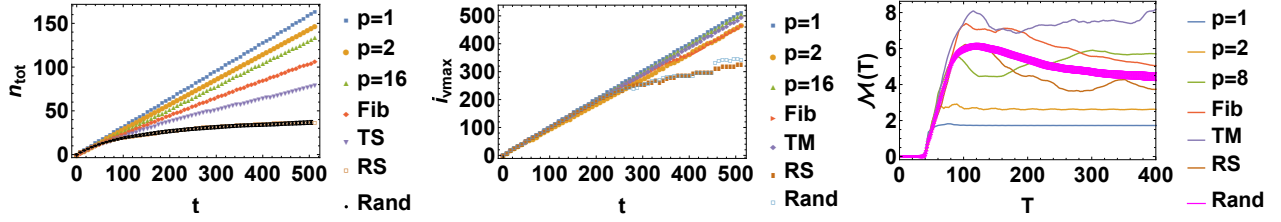


FIG. 13: (Colour online) Left:-Plot of $n_T = \sum_{i=L/2+1}^L c_i^\dagger c_i$ vs T in each of the distributions discussed in the paper. For the random sequence errorbars are shown as we have averaged over several realizations Middle:- Plot showing the position of the fastest particle in the system at time T . In this case only one realization of the random sequence was simulated. Right:- Plot of Mutual Information (\mathcal{M}) between two subsystems α and β where α consists of sites $L/2 + 1$ to $L/2 + 40$ and β consists of sites $L/2 + 41$ to $L/2 + 80$. For the random sequence case, the error bars are denoted by the thickness of the line. See text for details.

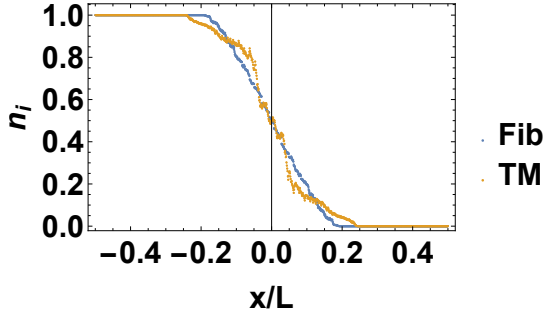


FIG. 14: (Colour online) A comparison of $n_i = \langle c_i^\dagger c_i \rangle$ vs $x = (i - L/2)/L$ for on site potentials arranged in Thue Morse and Fibonacci sequence at time $T = 500$. Rest of the parameters are same as Fig. 12. See text for details.

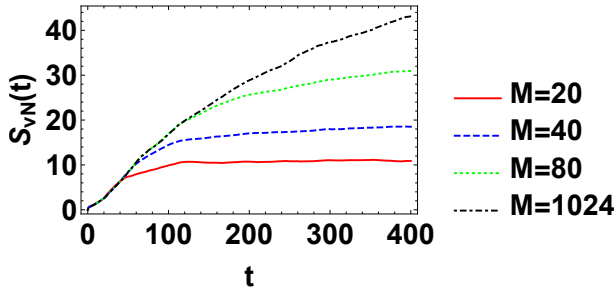


FIG. 15: Plot of Von Neumann entropy vs Time for a system in which the on site potential is distributed as $\mu + \delta\mu$ and $\mu - \delta\mu$ in a Rudin Shapiro sequence for various subsystem sizes M . The parameters are same as in Fig. 9. See text for details

as a random sequence. Since the system size considered, $L = 2048$ is large, a lot of self averaging occurs and averaging over $\sim 10^2$ ensembles is enough to create a dataset with small errorbars. In our plot we have averaged over 60 ensembles. The data agrees with all the features discussed about uncorrelated scattering events in the context of the Rudin Shapiro sequence.

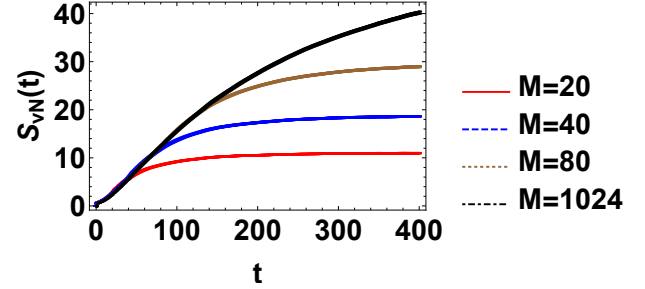


FIG. 16: (Colour online) Plot of Von Neumann entropy vs Time for a system in which the on site potential is distributed as $\mu + \delta\mu$ and $\mu - \delta\mu$ in a random sequence for various subsystem sizes M . The parameters are same as in Fig. 9. The error bars are within the thickness of the lines. See text for details

F. Breaking the thermodynamic limit

Fig 17 extends a result first shown by Alba and Heidrich Meissner¹. They showed for the TS systems, if you break the thermodynamic limit, particles bouncing back from the walls has an effect of increasing entropy once their trajectories cross each other at the center of the chain. We show how this result for four representative systems of small length $L = 128$. For the TS case, the step like structure is similar to what they showed. The explanation is similar, the jumps coincide with the particles reflected from the left and right boundaries crossing A , the left end of the subsystem. The first jump is approximately at $T = L$ as can be seen from the plot. Now when we break the translation symmetry, the particles undergo scattering from the potential landscape, which when the inhomogeneity becomes disorder becomes very large in number. The scatterings not only result in a reduction in particle density in $i > L/2$ but also force some particles to cross the boundary at $x = L/2$ back into the left half of the system before being pushed back again. This is what causes the generation of extra wavefronts. The two mechanisms are similar, in one more wavefronts are

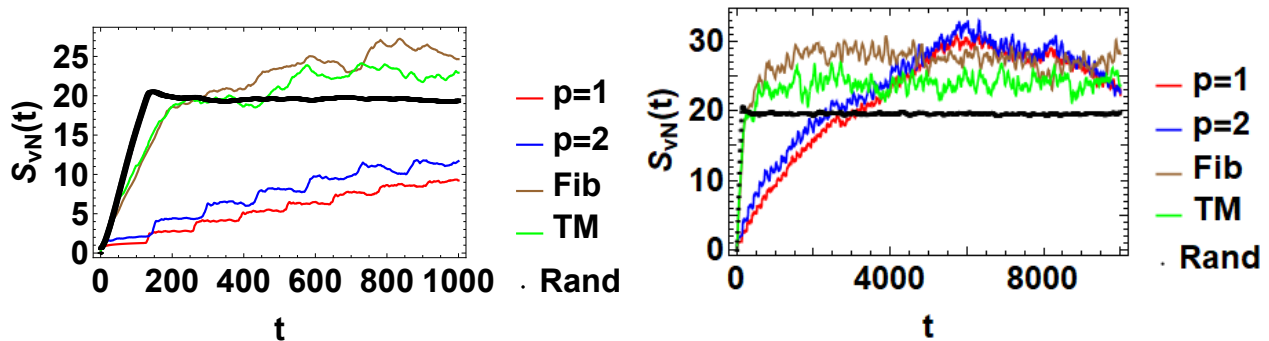


FIG. 17: (Colour Online) Left: Plot of S_{vN} vs T for four characteristic potentials, for a system of size $L = 128$, hence thermodynamic limit has been broken and particles are allowed to bounce off the boundaries. Right:- The same plot but for an even longer time scale. The thickness of the magenta line denotes the error bars of the Random potential data.

generated which cross the boundary at $x = 0$, in another the same wavefront under multiple reflections from the walls and crosses the boundary at $x = 0$ multiple times. The multiple crossings of the same wavefront is equivalent to creation of new wavefronts from scattering centres.

However Fig 17 also shows for extremely long times the trend that inhomogeneity results in higher Entanglement is reversed. This is to be expected as for very large times, the number of reflections of a particle matches the number of scattering events which the particle undergoes under the influence of homogeneity. With the number of wavefronts involved almost equal, the only decisive factor is the number density of particles present in the $i > L/2$ half of the system, which gives, as expected, higher Entanglement Entropy for the TS case. The plots also show, Quasi-Periodic potentials cause higher leakage of information at long times than fully disordered potentials. It has been shown that in integrable Quasi-Periodic systems scattering events occur as in the case of Anderson Localization³², but the scattering events are correlated instead of uncorrelated. The one-particle wavefunctions for such discrete quasiperiodic systems possess a multifractal structure with no mobility edge. Thus while there are a larger number of scattering events than the periodic case, localization does not occur and much larger particle density is present in $x > 0$ subsystem. Hence both the factors required to aid leakage of information is present in these systems. This results in these systems showing maximum information leakage for the inhomogeneous quench.

G. A peculiarity of the entanglement at high $\delta\mu$

Fig. 18 shows the half chain entanglement and in this case A is taken at site $i = L/2 + 1$. Here as expected, when we are in the low disorder limit, the Entanglement

increases with disorder until a maximum after which it

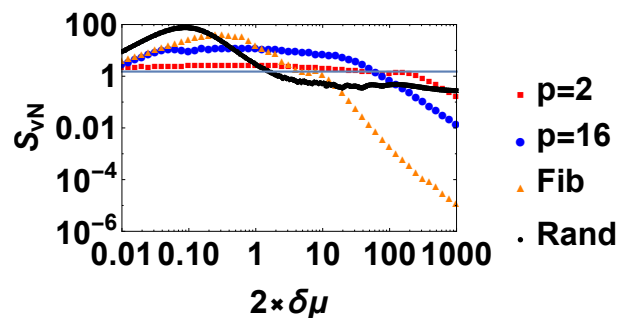


FIG. 18: (Colour online) Left:- Plot showing Von Neumann entropy vs strength of inhomogeneity denoted by $\delta\mu$ at $T = 500$ for different representative cases. The subsystem is of length $M = L/2$, and the position of A is at $i = L/2 + 1$. Right:- Same plot but with the position of A shifted to $i = L/2 + 21$ and hence $M = L/2 - 20$. The black dashed line denotes the Entanglement for $\delta\mu = 0$. The rest of the parameters are same as Fig 3. See text for details.

starts decreasing for all the cases of inhomogeneity. The random case shows the steepest ascent and descent compared to the other two cases. However at very high disorder Entanglement still stays at a finite value. This peculiarity is due to the fact that, for certain disorder realizations (which are extensive in number) a very small particle density can be present in the $x > 0$ sector. This effectively ensures a finite number of wavefronts reaching the subsystem and carrying information even with a low particle density. This raises the entropy. However, in cases where we have considered a periodic potential or a Fibonacci potential, correlated scattering events show no such peculiarity. Next as described in the main text, if we shift A to $x > 0$, the powerlaw decay is observed for the TS breaking potentials. In Fig. 19 we show this for a few characteristic cases. Understanding of the power laws for the different kinds of potential results is left for a future work.

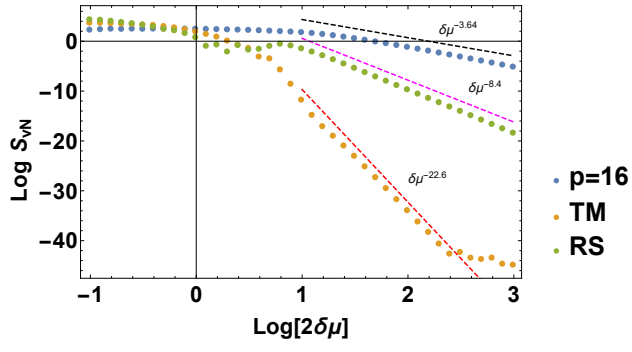


FIG. 19: (Colour Online) Plot of the same quantities as Fig 18, but with A at $i = L/2 + 10$. The dashed lines show the power law for the respective best fits. See text for details